Performance Assessment and Comparison of Two Types Linear Motors for Electromagnetic Catapult

Huilai Li*, Xiaomin Li, Zhiyuan Li
Mechanical Engineering College, Shijiazhuang, P.R. China, 050003
*Corresponding author, email: lihuilai_2013@163.com

Abstract

Linear motors are strong candidates in electromagnetic launching technology for space-use. In this paper, two types linear motors, including parallel magnetic circuit linear permanent magnet brushless DC motor (PMC-LPMBDCM) and serial magnetic circuit linear permanent magnet brushless DC motor (SMC-LPMBDCM), have been presented for electromagnetic catapult. The rudimental configurations of these two-types linear motors are researched respectively. Then the contrast of performance between PMC-LPMBDCM and SMC-LPMBDCM is investigated detailedly. The electromagnetic properties and thrust characteristics are researched by finite element analysis (FEA) and experiment. Simulated and measured results can provide useful references to select the suitable type of motor for electromagnetic catapult.

Keywords: electromagnetic catapult, parallel magnetic circuit linear permanent magnet brushless DC motor (PMC-LPMBDCM), serial magnetic circuit linear permanent magnet brushless DC motor (SMC-LPMBDCM), performance assessment

1. Introduction

The technology of electromagnetic launch is a newly developed linear propelling one, which uses electromagnetic force to launch the object and to be suitable for electromagnetic catapult applied to aircraft launch [1, 2]. Electromagnetic Aircraft Launch Systems (EMALS) use linear motors to accelerate aircraft to launch speed. It can obtain feedback information to determine aircraft position or velocity so as to adapt to variable loads and avoid load peak. Linear induction motor (LIM), linear permanent magnet synchronous motor (LPMSM) and linear permanent magnet brushless DC motor (LPMBDCM) are the three types that are frequently considered for use in EMALS [3, 4]. Usually, LIM is applied to heavy- mass aerocraft launch, because it can generate a larger thrust than the latter one. For permanent magnet type's linear motors, they are usually applied to relative low-mass unmaned aircraft vehicle (UAV) launch. LPMBDCM is a moving- magnet linear motor with a long primary section and a short secondary section. The double-side normal force could be counteracted each other, so the mover can avoid the impact of a unilateral magnetic pull.
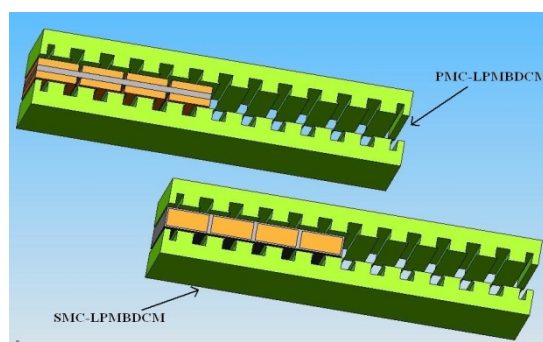

Figure 1. Basic Structure of Two Types Linear Motors

For electromagnetic launch applications, the double-side-stator structure of PMC-LPMBDCM and SMC-LPMBDCM are respectively shown in Figure 1. As their primary has to connect with the power supply cables, it is suitable for the demands of reliability. In this paper, performance assessment and comparison of two types of motors are evaluated using FEA method and experiment. The research of performance assessment of this thesis is to produce a method of synthesizing linear motor in such a way as to optimize its overall efficiency and performance.

2. Comparision of Model

The structural model of LPMBDCM is composed of permanent magnets in secondary and coil winding with slotted stator in long primary. Due to the different magnetization direction of permanent magnet on two sides, there are two types magnetic circuit: parallel magnetic circuit (PMC) and serial magnetic circuit (SMC), as shown in Figure 2 [2].
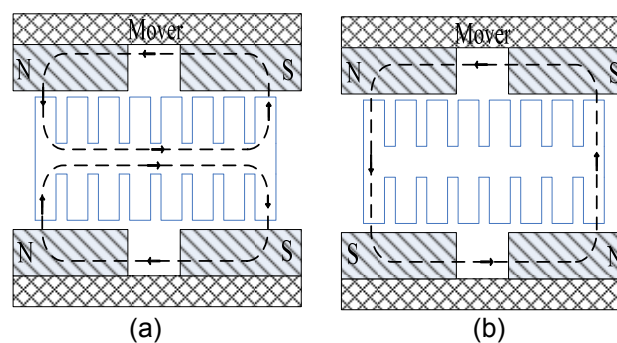

Figure 2. Two Types Magnetic Circuit (a) PMC, (b) SMC

The mechanism shell of PMC-LPMBDCM and SMC-LPMBDCM has the different structure with a moving-magnet type secondary, as shown in Figure 3.
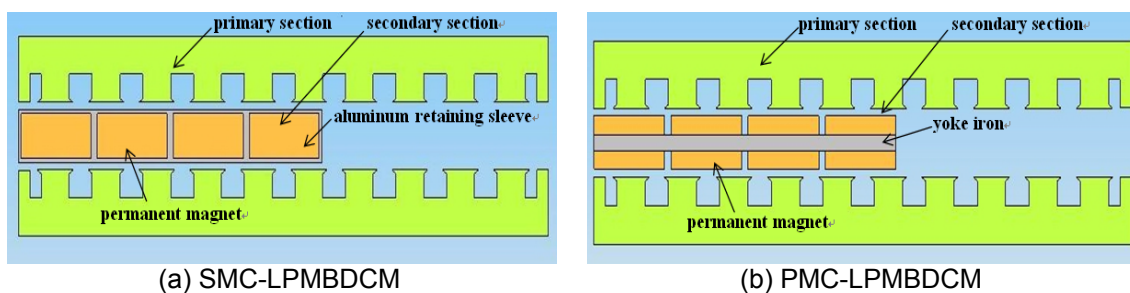

Figure 3. Two Types Linear Motors Configuration (a) SMC-LPMBDCM, (b) PMC-LPMBDCM

PMC-LPMBDCM has a moving-magnet type secondary, which composed of double-sided permanent magnets arranged by N face N direction, while the primary section is replaced by coil winding enveloped with lactoprene in the silicon-iron slots. However the single-sided permanent magnets of secondary section are arranged by N face S direction in a fixed aluminum retaining sleeve for SMC-LPMBDCM. In order to increase the thrust force and balance the applied torque, the linear motor is usually designed as double-side structure and short-range distributed winding.

3. Finite Element Analysis
3.1. Air-Gap Magnetic Field Calculation
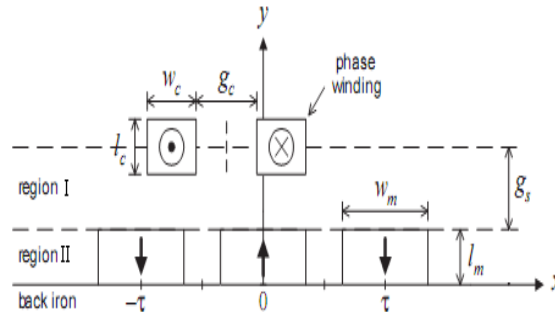For the air-gap magnetic field calculation, the model under consideration is shown in Figure 4.

Figure 4. Two Regions Defining the Problem

According to Figure 4, assumption that (i) the stator is infinitely long in the *x*-direction; (ii) the current is only along *z*-direction; (iii) the permeability of the back iron is infinite. Under these assumptions, the characteristic equations of each region are given as follows:

$$\begin{cases} \dfrac{\partial^2 A_2}{\partial x^2} + \dfrac{\partial^2 A_2}{\partial y^2} = -\mu_0 J & Regin \ \mathrm{I} \\ \dfrac{\partial^2 A_1}{\partial x^2} + \dfrac{\partial^2 A_1}{\partial y^2} = 0 & Regin \ \mathrm{II} \end{cases} \tag{1}$$

Where *A* is a curl of magnetic vector and variable *J* is the equivalent-magnetizing-current. Boundary conditions that must be satisfied between two regions are:

$$\begin{cases} B = \nabla \times A \\ \nabla \times \left(\dfrac{1}{\mu} \nabla \times A \right) = J \end{cases} \tag{2}$$

Where *K* denotes surface current density and $\hat{n}$ is a unit vector normal to boundary surface from region Ⅱ to region Ⅰ. Boundary conditions (1) specialize to:

$$\begin{cases} H_{1x} = 0 & , \ y = g_s \\ H_{1x} = H_{2x} \ \ and \ \ B_{1y} = B_{2y}, \ y = l_m \\ H_{2x} = 0 & , \ y = 0 \end{cases} \tag{3}$$

The proposed model is validated by FEA simulation. The saturable M19 steel is assumed for back iron material and the permeability of PM material is assumed to be $1.05\,\mu_0$ with B_r=1.6T. The prototypal parameters are as follows: 10 pole pair and 60 slots, current density 100A/mm^2 and 2 pairs of mover. The pole pitch (τ), length of air-gap (g_s), size of slot dimension (w_c, l_c, h_s), size of PM dimension (w_m, l_m, h_m), and the length of primary and secondary section (L_p, L_s) should be adjusted properly. Some motor parameters and PM characteristic have been shown in Table 1.

Table 1. Motor Design Data and PM Characteristic

Symbol	Item	Value
τ	pole pitch	120mm
g_s	length of air-gap	2mm
w_c	width of slot	15mm
l_c	length of slot	20mm
h_s	depth of slot	90mm
w_m	width of PM	60mm
l_m	length of PM	80mm
h_m	thickness of PM	12mm
L_p	primary length	2.5m
L_s	secondary length	235mm
PM	material	Nd-Fe-B

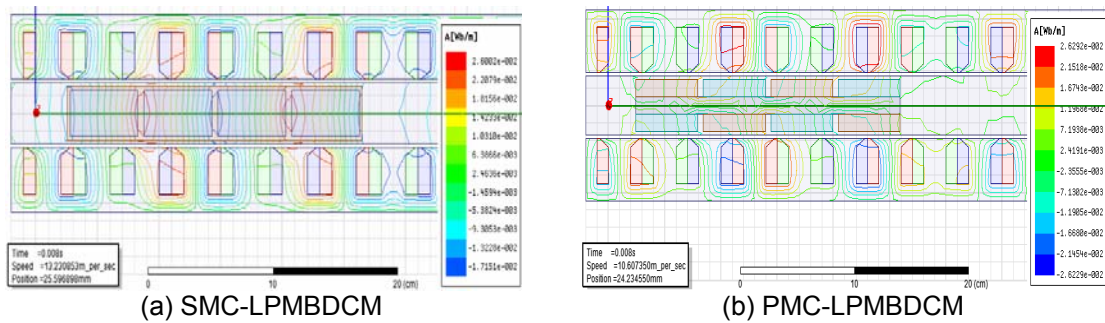(a) SMC-LPMBDCM   (b) PMC-LPMBDCM

Figure 5. Distribution of Flux Linkage

The flux linkage distribution for each linear motor are shown in Figure 5(a) and Figure 5(b), respectively. It can be seen that the magnetic-force-line in PMC-LPMBDCM is parallel and the magnetic circuit structure is more complex than that of in SMC-LPMBDCM. As the magnetic permeabilities of applied materials are different, most of magnetic line thread through silicon-steel tooth and air-gap to form double-sided parallel circuit in PMC-LPMBDCM. The magnetic circuit of PMC-LPMBDCM has a symmetrical form in bilateral air gap by contrast with that of SMC-LPMBDCM, which its bilateral stator makes the magnetic flux lines formed into a single magnetic circuit in the air gap. Moreover, as the reasons of end effect and magnetic leakage, the density of magnetic flux is different along the stator, and the flux density in yoke iron and silicon-steel tooth section is relative larger than that of in other section.
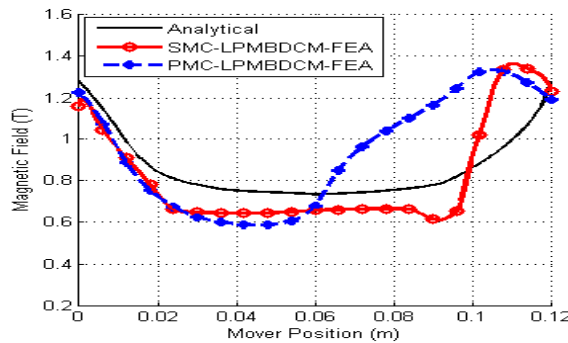

Figure 6. Mover Position under Different Magnetic Field

Figure 6 shows the plot of the magnetic field over the surface of the shuttle for a pole pitch distance. The shuttle sweeps from left to right with a certain slip speed. As the effect of back electromotive force (back-EMF), the field strength at the surface of the shuttle decreases

due to the induced opposing field. The magnetic field strength wave shape of PMC-LPMBDCM and SMC-LPMBDCM are approximated trapezoidal wave. This is because the opposing magnetic field caused back-EMF and the end effect.

3.2. Eddy Current Field Calculation and Results

Simulation results show that the average eddy-current loss is 835W in 0.2 second time on PMC-LPMBDCM and the computational value is 624W on PMC-LPMBDCM. To explore the influencing factor of eddying current force in the launch, two simulation studies are performed on SMC-LPMBDCM.First simulation condition: under the condition of non-current in the winding coil and setting the mover an constant velocity of 20m/s, only the spatial harmonic magnetic field has been considered for eddying current force. Second simulation condition: the permanent magnet of NdFeB material is converted to air as a comparison with what considered above, and also a three-phase excitation current with rich harmonic is applied in the windings, as shown in the formula (4). Set the mover a velocity of 20m/s, only the armature reaction has been considered for eddying current force.

$$i_A = 0, \quad i_B = 600A, \quad i_B = -600A \tag{4}$$

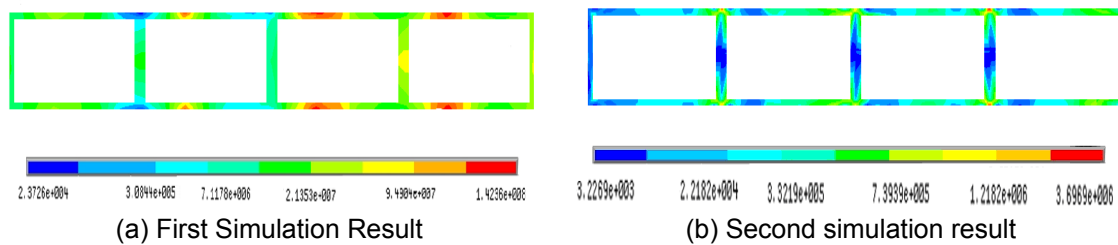(a) First Simulation Result   (b) Second simulation result

Figure 7. Distribution of Eddy Current of Different Simulations

Figure 7 shows the distribution of eddy current *Jz* for two simulation results. As can be seen from the figure, the eddy current filed is almostly induced by the internal magnetic field of permanent magnet in slotted structural stator. The eddy-current force in the retaining sleeve induced by the slotted structural stator is more larger with a order of magnitude than that of induced by the large current of armature reaction, and the former is more widely distributed. The results shows that the slotted structural stator is the main factor to make eddy-current force for high-speed linear motor.
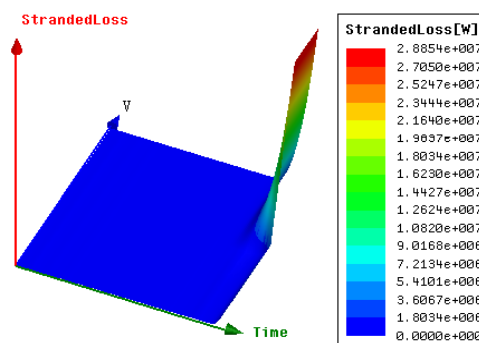

Figure 8. Relationship between Stranded Loss, Velocity and Time

The eddy current resistance force seems to be importantly related with the velocity. This can be equally observed in Figure 8. Showing the relationship between peak value of

standedloss *P* and velocity and time for SMC-LPMBDCM. When the velocity and time increased to a certain value, the stabdedloss *P* will suddenly increase with a exponential variation.

3.3. Thrust Fluctuation Calculation and Results

A model of volt-control commutation is built to analyze the thrust performance using Simulink. In order to compare the thrust output for two types motors, the thrust characteristics is discussed. The detail parameters are presented as follows: number of pole-pairs *P* is 4, the coil inductance *L*=80mH, phase resistance *R*=0.0455Ω, actuating voltage *U*=600V, shuttle mass *m*=30kg.
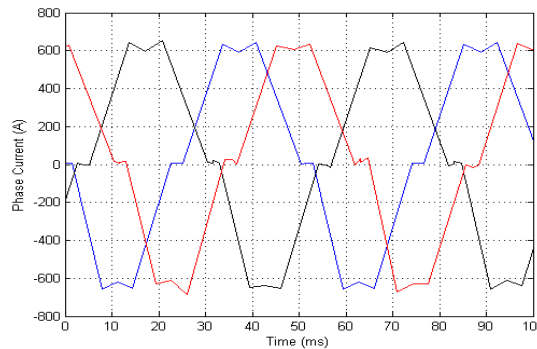

Figure 9. Actuating Current Wave

Due to the high similarity of primary for two types motors the current waveforms in winding coil are substantially the same, as shown in Figure 9. It can be seen that they are periodic trapeziform wavesforms and the top waveforms of the current fall slightly. Thrust ripple can be defined as the ratio of peak-to-peak amplitude to average thrust shown in form (5).

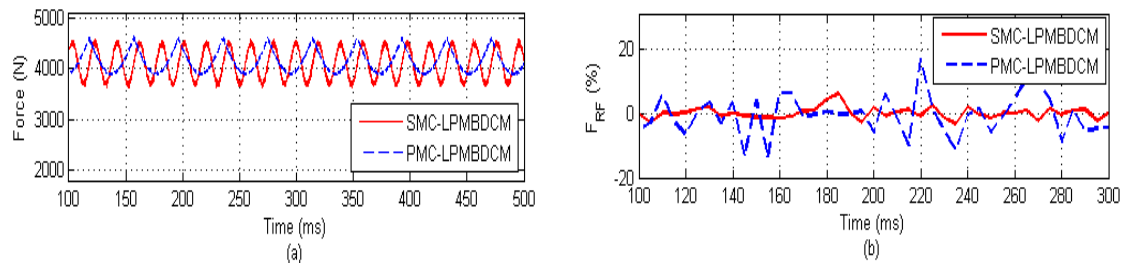$$F_{RF} = \frac{\Delta F_{pp}}{F_{av}} \times 100\% \tag{5}$$

Figure 10. Simulation Results of Different Thrust Force

The thrust output and thrust ripple results have been shown in Figure 10(a) and (b), respectively. It can be seen that PMC-LPMBDCM has a better performance on thrust characteristic. Not surprisingly, from the research of air-gap magnetic field discribed above, the density of magnetic field and the length of air-gap in the *x*-direction can influence the thrust force, thus PMC-LPMBDCM can generate a relative larger thrust output. The thrust fluctuation is mainly generated by the phase conversion. The thrust fluctuations caused by the end effect and cogging thrust is very small in the total proportion.

4. Performance Analysis of Two Types Linear Motors
4.1. Maximum Thrust Force Analysis

One concerned assessment is how to obtain maximum average force. This question can be optimized by some analysis and simulation in order to find magnitude- constrained currents that maximize the magnitude of thrust force [2]. The maximum thrust force output can be stated as follows.

Maximize $f(x, u)$

Subject to, $\left| u_j \right| \leq U, j = 1, 2, 3$

$x \in (0, 2\tau)$

The sign of the objective function is chosen in order to match the desire force sign. Note that the current limit must be considered for finite current input and u_j is given to produce continuous maximum thrust force.The emphases of solving objective function above-mentioned is maximum average force F_a, which is determined according to:

$$F_a = \frac{1}{2\tau} \int_0^{2\tau} f^*(x)dx$$

$$= \frac{1}{2\tau} \int_0^{2\tau} \frac{d\lambda_s^T(x)}{dx} i + \frac{1}{2} i^T \frac{d\psi(x)}{dx} i \, dx \qquad (6)$$

One emphasis parameter is the maximum average force to compare the two types motors. One design is better than another design if, for the same moving mass, its value of F_a is higher because it can produce higher force and higher acceleration [5].

4.2. Minimum Copper Loss Analysis

The next optimal optimization design is to find magnitude-constrained currents that minimize the power dissipation due to copper loss and iron loss. The total average power dissipation is defined as:

$$P_x = \frac{R}{2\tau} \int_0^{2\tau} \tilde{i}^T \tilde{i} \, dx \qquad (7)$$

Where τ is the magnet pitch, R is resistance, i is current value. Square wave current can be considered as the aggregate of various harmonics currents. In order to gain the maximum quotient of thrust force versus current, the fundamental current in coil winding must be synchronizing with back-EMF. However, the current waveshape always lags the terminal voltage due to armature reaction. The phase conversion needs to be done in advance. The advance commutation angle, which caused fundamental current synchronizing with back-EMF, is defined as:

$$\alpha = \arctan(\frac{kL_s i_s v^2}{K_e} + R_s i_s) \qquad (8)$$

Where v is the velocity, L_s and R_s are the inductance and resistance separately, K_e denotes the back-EMF coefficient.

The minimum loss problem is concerned with advance commutation angle for PMC-LPMBDCM and SMC-LPMBDCM. This problem may be posed as an optimization problem to determine the different optimal advance electrical angle for two type's linear motors [6, 7].

4.3. Results and Discussion

The maximum thrust force question is researched to obtain maximum acceleration. Considering the current constraint condition acted on two type's linear motors, the relationship of maximum average force versus current value is shown in Figure 11.
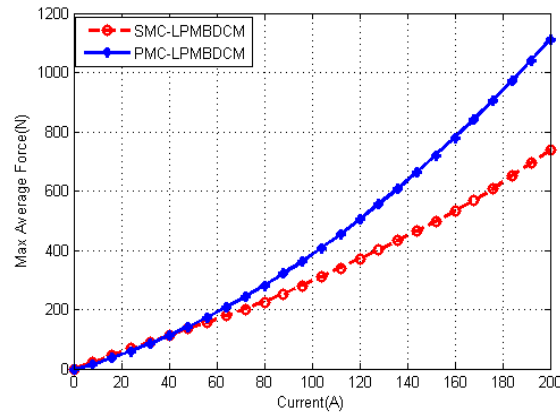
Figure 11. Relationships between Max Average Force and Current Value

It can be seen that the same maximum average force output, PMC-LPMBDCM needs less feed current than that of SMC-LPMBDCM. One can notice that the difference is not visible, when the current value is small. When the current value is greater than 100A, the performance between SMC-LPMBDCM, PMC-LPMBDCM will be presented.
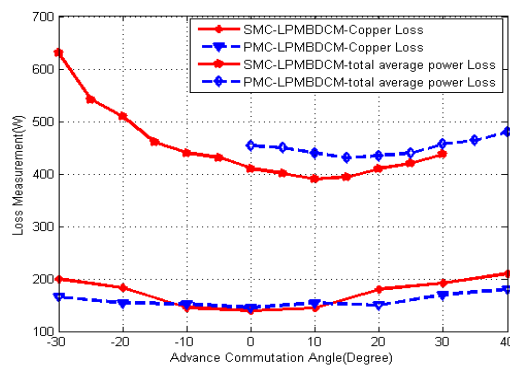

Figure 12. Relationships between Loss Measurement and Advance Commutation Angle

Figure 12 shows that the loss measurement vs. advance commutation angle under magnitude constrained currents for two types of motors. It can be seen that the transformation trends of copper loss and total average power dissipation for SMC-LPMBDCM are the same as that of PMC-LPMBDCM. However, the total average power dissipation of PMC-LPMBDCM is a little larger than that of SMC-LPMBDCM. These results can be explained that the iron loss in iron yoke may be larger than that of in the aluminum retaining sleeve. When the advance commutation angle is 10 degrees, the total average power dissipation is minimum. The copper loss and total average power dissipation of LPMBDCM are minimum as advance commutation angle is 15 degrees.

5. Experiment and Results

Figure 13 shows the prototype machine of a subscale long-primary LPMBDCM. The rated power of linear motor for experiment is 4 kW, 300 V. To validate the simulated results above, the secondary sections of PMC-LPMBDCM and SMC-LPMBDCM are manufactured to execute relational experiment.

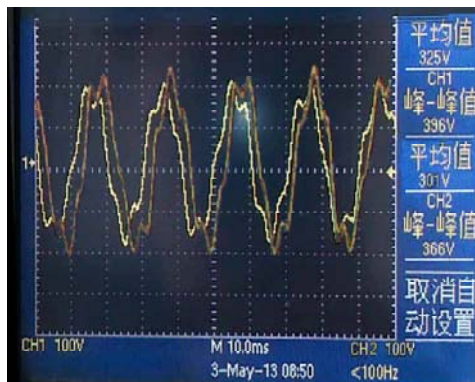Figure 13. Experimental Machine of a Subscale Long-primary LPMBDCM

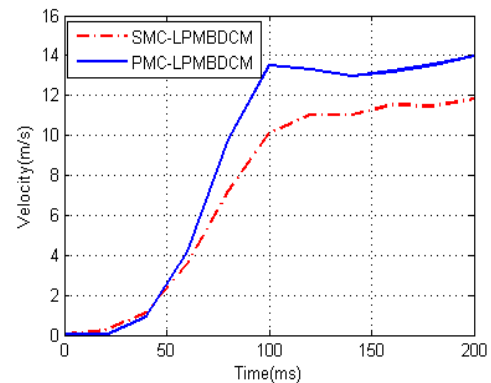Figure 14. Waveforms of Measured Back-EMF

Figure 15. Measured Velocity of Mover

Figure 14 shows the waveform of measured back-EMF and the measured mover vocility for two types motors has been shown in Figure 15. As can be seen from Figure 14, the average back-EMF voltage is 325 V on PMC-LPMBDCM, which is bigger than that of on SMC-LPMBDCM with a value of 301V. From the measured results, it can be observed that the experimental results for prototype match with the simulation results. As can be seen from the Figure 15, the velocity output of PMC-LPMBDCM is greater than SMC-LPMBDCM in the same configuration. The electromagnetic launch for prototype works in the short-term system. The whole transient acceleration process with high current density and high thrust achieved in approximately 0.15 second. It is worth to mention that the experimental results were obtained in the first prototype before advance commutation control applied, so the practical systems also have the chance to improve the performance output.

6. Conclusion

EMALS has the advantages of high thrust, good controllability, etc. PMC-LPMBDCM and SMC-LPMBDCM are two candidates commendably applied to UAV launch. The model analysis of two types linear motors is analyzed in this paper. Then the similarities and performance characteristic are investigated for two types linear motors, including mechanism, air-gap magnetic field distribution, eddy current resistance force and thrust fluctuation, with an emphases of maximum thrust force and minimum loss question. The results show that PMC-LPMBDCM has a higher thrust output characteristic, which seems to be a better choice under small fluctuation condition.

References

[1] MR Doyle, DJ Samuel, T Conway, RR Klimowski. Electromagnetic aircraft launch systems- EMALS. *IEEE Trans.* Magn., 1995; 31(1): 528–533.

[2] D Patterson, A Monti, C Brice, T Bertoncelli. *Design and simulation of an electromagnetic aircraft launch system,* in 37th IAS Annu. Meeting. 2002; 3: 1950–1957.

[3] Gorazd Stumberger, Damir Zarko, Mehmet Timur Aydemir and Thomas A. Lipo. *Design and Comparison of Linear Synchronous and Linear Induction Motor for Electromagnetic Aircraft Launch System*. IEEE International Electronic Machines and Drives Conference, MADISON. 2003; 1: 494-500.

[4] Junyong Lu, Weiming Ma. Research on two types of linear machines for cover airstrip electromagnetic catapult. *IEEE Trans. Plasma Sci.,* 2009; 39: 105–109.

[5] Nattapon Chayopitak. Performance assessment and design optimization of linear synchronous motors for manufacturing application, Dissertation. Georgia institute of technology. 2007.

[6] Kou BaoQuan, Huang XuZhen, Wu Hong-xing. Thrust and thermal characteristics of electromagnetic launcher based on permanent magnet linear synchronous motors. *IEEE Trans. Magn.,* 2009; 45: 358–362.

[7] M Mirzaei, SE Abdollahi, A Vahedi. Permanent magnet dc linear motor for aircraft electromagnetic launcher,*14th Conf. Electromagnetic. Launch Technology*. Vancouver, BC, Canada. 2008: 1–6.

[8] Yan-Peng Sun, Shi Zhang, Xiao-He An, Hong-Peng Sun. Characteristics of Electromagnetic Pulse Coupling into Annular Apertures*. TELKOMNIKA Indonesian Journal of Electrical Engineering*. 2013; 11(11): 6848-6854.

[9] Lanxiang Zhu, Yaowu Shi, Yiran Shi, Life Deng, Hongwei Shi. Electromagnetic Vector Sensor array parameter estimation method*. TELKOMNIKA Indonesian Journal of Electrical Engineering*. 2013; 11(5): 2860-2868.

[10] Liu Mingdan, Chen An Jun, Wang Yong, Tan Pengfei, Zhao Sifen. Research on the Pulsed Magnetic Field Device for Sterilization of Fruit and Vegetable Equipment. *TELKOMNIKA Indonesian Journal of Electrical Engineering*. 2013; 11(4): 2084-2087.